

Multilevel Raised-Cosine Pulses for Data Transmission

Mohammad Alsharif

Department of Electrical Engineering, College of Engineering, Taif
University, Taif, Saudi Arabia.

Abstract

Multilevel raised-cosine pulses are defined and presented for use as a modulation technique. The detection of these pulses over an AWGN channel is examined, and optimal receiver architectures for coherent detection are derived. Closed-form expressions for the symbol error probabilities associated with these receivers are obtained. Optimal 2-, 4-, and 8-level coherent raised-cosine systems that minimize symbol error rates are identified. The performance of coherent multilevel raised-cosine systems is compared with that of corresponding conventional M-ary digital modulation schemes. Furthermore, the influence of additional factors, such as pulse duration, on system performance is investigated.

Keywords: Raised Cosine Pulses, modulation, optimum receiver, normalized correlation, error probability, AWGN.

1 Introduction

Raised-cosine signals are widely recognized for their spectrally compact characteristics, which makes them bandwidth-efficient. They are commonly employed for pulse shaping to reduce occupied bandwidth while keeping implementation cost low. Moreover, raised-cosine shaping has been proposed as a mean to mitigate excessive spectral spreading and improve energy concentration in various applications. In Rjeb et al.(2022), the paper proposes and designs novel multicore few-mode optical fibers based on raised cosine and trenched raised-cosine refractive index profiles to enable high-density space-division multiplexing (SDM). The designed fibers support seven cores, each carrying six spatial modes with large effective mode area, low differential mode delay, and significantly reduced inter-core crosstalk. These characteristics make the proposed fibers strong candidates for next-generation short- and medium-range high-capacity SDM optical communication systems. The authors in Gupta and Gamad (2022) analyze the symbol error rate (SER) performance of Generalized Frequency Division Multiplexing (GFDM) using root-raised-cosine (RRC) pulse-shaping filters under AWGN and zero-forcing detection. Simulation results show that varying the RRC roll-off factor significantly affects noise enhancement and SER, with lower roll-off values providing improved spectral efficiency and reduced inter-symbol interference. The study highlights the suitability of GFDM with RRC filtering for 5G applications requiring low out-of-band emissions and high data-rate reliability. The paper in Simon and Alouini (1999) derives exact expressions for the average bit error probability (BEP) of noncoherent M-ary orthogonal modulation (M-FSK) with square-law combining over generalized multipath fading where paths can be non-identically distributed and even follow different fading models. The key result is a finite-range integral whose integrand depends on the moment generating function (MGF) of the combined SNR, enabling efficient numerical evaluation. Using plots (e.g., Figs. 1-5), the authors show that non-uniform multipath intensity profiles (MIP) and fading correlation profiles (FCP) can significantly degrade BEP and must be modeled for accurate performance prediction. In Singh et al. (2019), the paper evaluates BER performance of M-QAM (16/64/256/1024) under AWGN while comparing binary vs Gray coding, raised-cosine pulse shaping, and convolutional coding across oversampling factors 1-5. Results show Gray coding reduces BER relative to binary coding, and raised-cosine pulse shaping mitigates ISI effects; however, BER generally worsens with higher QAM order due to denser constellations, while oversampling changes SNR per the E_b/N_0 relation. The study links BER/SNR trends to spectral efficiency trade-offs, emphasizing that higher-order QAM increases throughput but requires higher SNR to maintain error performance.

In [Abeysekera \(2015\)](#), The authors propose a low-complexity CPM demodulator that performs symbol detection via iterative DFT-based frequency estimation for full-response raised-cosine (RC) CPM, avoiding matched-filter/Viterbi complexity and remaining independent of modulation index. Using CRB-based analysis and simulations, it shows that a few iterations remove DFT bias and yield frequency estimates approaching the Cramér–Rao bound, leading to BER close to noncoherent matched filtering (Fig. 4). Robustness tests with frequency/phase offsets demonstrate the proposed receiver maintains comparatively stable BER under severe phase variations (Fig. 5), making it attractive for phase-unstable channels (e.g., underwater links). In [Yilmaz and Kucur \(2009\)](#), the paper derives closed-form/computable SER expressions for M-ary QS-CDMA with maximal-ratio combining (MRC) over frequency-selective, time-nonspecific multipath generalized-gamma (GG3) fading, for arbitrary deterministic spreading sequences and chip-limited chip waveforms (rectangular, half-sine, raised-cosine). It shows that chip waveform affects performance mainly through MAI (via partial autocorrelation functions) and introduces Partial Power Ratio (PPR) as a waveform-selection metric; raised-cosine achieves the best SER because it yields the highest PPR and lower effective interference. Numerically/simulations indicate QS-CDMA can match or slightly outperform

synchronous CDMA without extremely tight timing—e.g., acceptable max quasi-synchronous delays around 0.2 (rectangular), 0.6 (half-sine), 0.7 chips (raised-cosine) depending on path power decay. In [Wang et al. \(2025\)](#), the paper proposes M-ary Spread Multiple Access (MSMA) for uplink cellular systems, where users are distinguished using a joint design of spreading codes and multi-user superposition constellations, and each user’s bits are mapped across multiple subcarriers to harvest frequency diversity (Figs. 1–6). At the receiver, M-ary code de-mapping via generalized sphere decoding (GSD) is used to balance multi-user interference and diversity gain, yielding lower BER than PD-NOMA at the same overload ratio and outperforming SCMA in high E_b/N_0 while supporting higher overload (Figs. 8–11). In [Biswas et al. \(2020\)](#), the paper investigates a digital link using 256-QAM with (square-root) raised-cosine pulse shaping over an AWGN channel, comparing BER/SER performance with and without filtering. MATLAB simulations indicate that adding the RRC/SRRC filter reduces ISI-driven degradation and improves BER/SER relative to unfiltered transmission, supporting higher-rate QAM operation. In [Lin et al. \(2021\)](#), the authors design collocated MIMO radar phase-coded waveforms while explicitly including a raised-cosine (square-root raised-cosine) filter to reduce spectral leakage in practical implementations. It formulates an optimization that jointly controls beam pattern mismatch and auto/cross-correlation side lobes, and shows numerically that good two-peak beam patterns and low side lobes are achievable after filtering. Also, raised cosine pulses have been used in other applications such as image and video processing. In [Deivalakshmi et al. \(2017\)](#), the paper proposes Raised Cosine Adaptive Gamma Correction (RC-AGC), a global contrast-enhancement method for dark images/low-light videos that applies a raised-cosine envelope to the adaptive gamma parameter derived from a weighted histogram CDF. Experiments show RC-AGC suppresses transformation-function spikes (reducing artifacts) and improves objective/subjective quality metrics (e.g., HFM/PSNR/UQI) versus several histogram-modification base-lines, with low computational cost. In [Boes et al. \(2015\)](#), the authors experimentally compare raised-cosine shaped versus NRZ rectangular-pulse complex-modulated signals for an all-electrical MMIC E-band (77 GHz) point-to-point link over 4.1 km, demonstrating up to 12 Gbit/s in 4.05 GHz RF bandwidth. Raised-cosine shaping improves spectral confinement (less out-of-band leakage) but shows higher sensitivity to linear/nonlinear effects and sampling timing, leading to worse EVM/BER than rectangular pulses in their setup. Other applications for raised cosine pulses include radar systems. In [Willstatter and Zoltowski \(2022\)](#), the paper proposes the usage of a square-root raised-cosine (SRRC) frequency-domain pulses (inspired by OTFS & “frequency-domain cyclic prefix” ideas) as Doppler-tolerant radar waveforms, analyzing them via the auto-ambiguity function. The resulting ambiguity surfaces exhibit a ridge along zero delay (reduced delay “Doppler coupling compared with LFM) and lower out-of-band side lobes, and the authors discuss practical truncated approximate implementations (e.g., envelope tracking amplification) with noted energy/peak-power trade-offs. The paper is arranged into five sections. Section II describes and illustrates multi-level raised-cosine signals, while Section III focuses on coherent detection and the associated performance analysis. Section IV compares these signals with conventional modulation methods, and Section V provides the conclusion.

2 Multilevel Raised Cosine Signals

The multilevel raised-cosine-modulated (MLRC) pulses can be expressed in the general form as:

$$T(t) = \sqrt{\frac{2E_s}{T_s}} \cos(w_c t + \Theta(t) + \alpha), \quad 0 \leq t \leq T_s \quad (1)$$

where E_s denotes the symbol energy over a symbol interval of duration T_s seconds, w_c is the angular carrier frequency, $\Theta(t)$ represents the information-bearing phase and α is the initial phase at ($t = 0$). The information carrying phase $\Theta(t)$ for MLRC pulse is given by:

$$\Theta(t) = mF(t), \quad 0 \leq t \leq T_s \quad (2)$$

where m is the digital data taking one of the values $\pm 1, \pm 3, \dots, \pm(M - 1)$. The phase function $F(t)$ is given by:

$$F(t) = \begin{cases} \frac{1}{2LT_s} \left[1 - \cos\left(\frac{2\pi t}{LT_s}\right) \right] & 0 \leq t \leq T_s \\ 0, & otherwise \end{cases} \quad (3)$$

and $f_m(t)$ represents the instantaneous frequency as a function of time and it is defined as $f_m(t) = 2\pi \int_0^t F(\nu) d\nu$. For MLRC signaling:

$$f_m(t) = \begin{cases} \frac{\pi t}{LT_s} - \frac{1}{2} \sin\left(\frac{2\pi t}{LT_s}\right), & 0 \leq t \leq T_s \\ 0, & otherwise \end{cases} \quad (4)$$

L denotes the signal length, assumed to be 1, while T_s represents the symbol duration in seconds.

3 Detection and Performance

The detection of MLRC pulses can be approached by formulating it as multi hypothesis testing problem, where each hypothesis corresponds to one possible transmitted pulse. The hypothesis test is given by:

$$\left. \begin{array}{l} H_1 : r(t) = T_1(t) + n(t) \\ H_2 : r(t) = T_2(t) + n(t) \\ \vdots \\ H_M : r(t) = T_M(t) + n(t) \end{array} \right\} \quad 0 \leq t \leq T_s \quad (5)$$

The M modulated MLRC pulses are denoted by $T_1(t) \dots T_M(t)$, while $n(t)$ represents the additive white Gaussian noise with a one-sided power spectral density

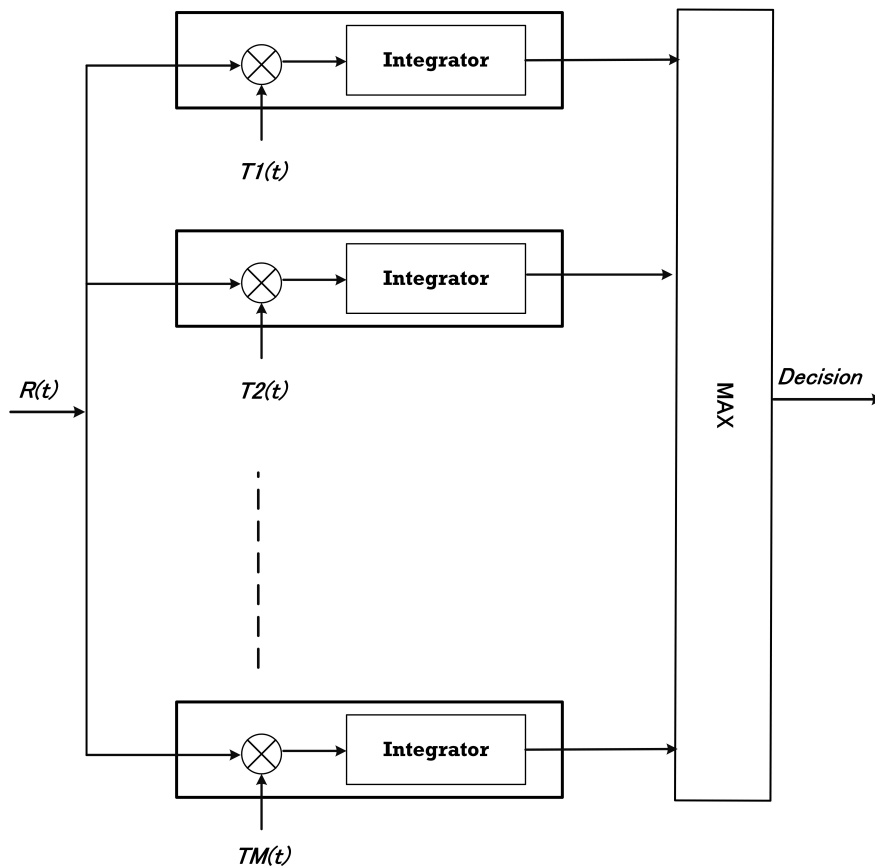


Fig. 1 Optimum receiver of MLRC pulses

of N_0 watts/Hz. Fig. 1 shows the optimum receiver of MLRC pulses. The detection problem consists of observing the received MLRC pulses in noise and optimally determining which of the M MLRC pulse was transmitted.

4 Results

The error rate performance of the binary MLRC pulses using the optimum receiver is shown in Fig. 2. In the same figure, the performance of BPSK and binary orthogonal FSK is presented. It can be observed that binary MLRC modulation performs about 0.8 dB worse than binary orthogonal FSK and nearly 4 dB worse than BPSK for error rates up to 10^{-6} . Despite this, MLRC modulation is less complex than binary orthogonal FSK, making it suitable for applications where system simplicity is prioritized over bit error rate performance. Additionally, the bandwidth efficiency of the binary MLRC system surpasses that of other modulation schemes, offering an advantage in scenarios where some degradation in error performance is acceptable in exchange for improved bandwidth efficiency.

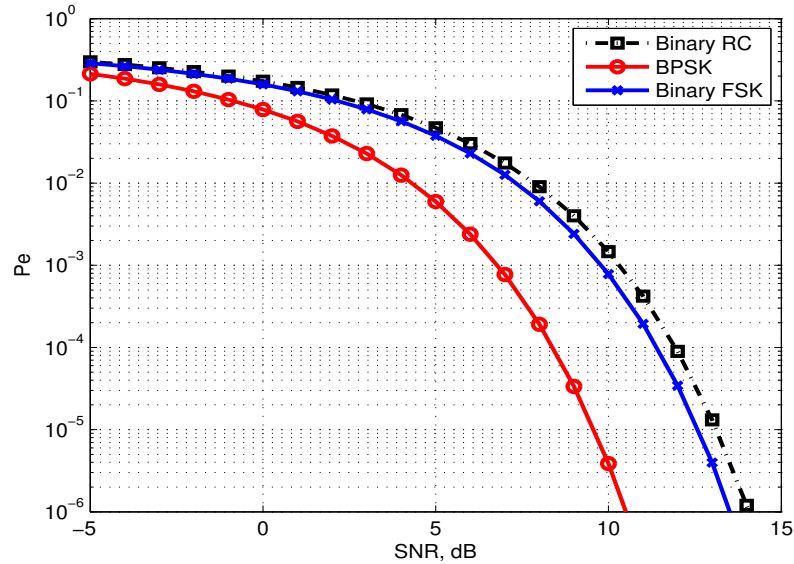


Fig. 2 Error probability performance of binary MLRC pulses, BPSK and FSK

Similarly, Figure 3 shows the performance of the quad MLRC, 4-PSK, and 4-FSK systems. Here, the quad MLRC system is approximately 1 dB worse than 4-FSK and about 4 dB worse than 4-PSK at an error rate of 10^{-6} .

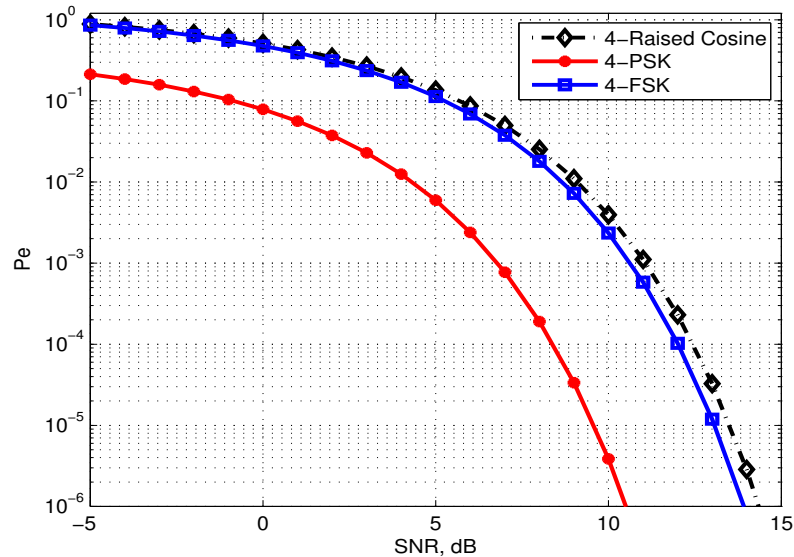


Fig. 3 Error probability performance of quad MLRC pulses, 4-PSK and 4-FSK

Figure 4 presents the performance of the eight MLRC pulses, alongside 8-ary PSK and 8-ary orthogonal FSK. It can be seen that for SNR values above 10 dB, the eight MLRC pulses exhibit performance nearly identical to that of both 8-ary PSK and 8-ary FSK.

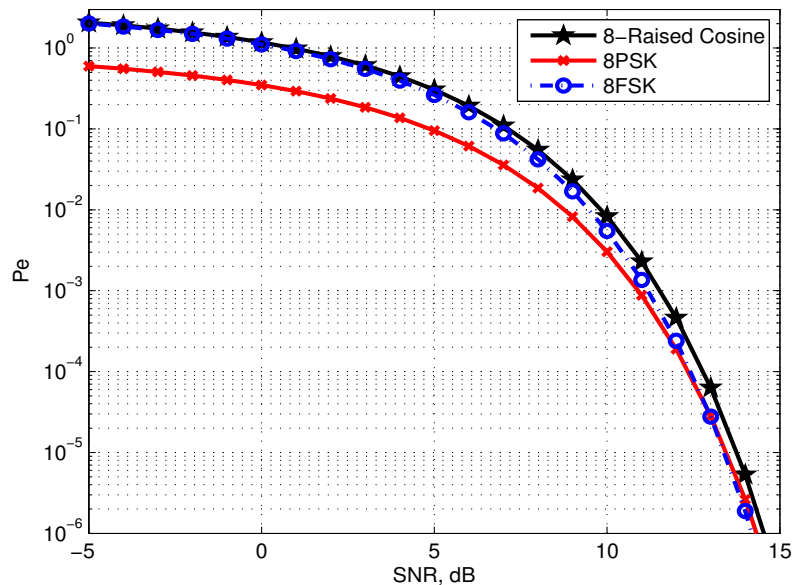


Fig. 4 Error probability performance of eight MLRC pulses, 8-PSK and 8-FSK

5 Conclusion

In this paper, theoretical expressions for error probability have been derived to evaluate the performance of MLRC pulses. These pulses are compared with other well-known modulation schemes. It is observed that binary MLRC pulses perform very similarly to binary FSK, while quad MLRC pulses achieve nearly the same performance as 4-FSK. Likewise, the eight MLRC pulses exhibit performance almost identical to 8-PSK and 8-FSK. Notably, as the modulation order increases, the performance of MLRC pulses approaches that of conventional techniques, highlighting their advantage for high-order transmission applications.

References

Abeysekera SS (2015) Robust full response m-ary raised-cosine cpm receiver design via frequency estimation. IEEE, ISBN: 978-1-4799-8058-1

- Biswas P, Rathore S, Khan MR, et al (2020) A novel approach of digital communication using 256qam and raised cosine filter. In: International Conference on Communication and Signal Processing (ICCSPPS). IEEE, July 28–30, 2020, India; ISBN: 978-1-7281-4988-2
- Boes F, Antes J, Meier D, et al (2015) Performance comparison of raised cosine shaped and rectangular pulsed signals in e-band wireless communication systems. In: 2015 IEEE Radio and Wireless Symposium (RWS). IEEE, 978-1-4799-5507-7
- Deivalakshmi S, Saha A, Pandeewari R (2017) Raised cosine adaptive gamma correction for efficient image and video contrast enhancement. In: 2017 IEEE Region 10 Conference (TENCON). IEEE, pp 2363–2368
- Gupta M, Gamad RS (2022) Symbol error rate analysis of generalized frequency division multiplexing in pulse shaping root raised cosine filter. In: 2022 IEEE 11th International Conference on Communication Systems and Network Technologies (CSNT), pp 647–650, <https://doi.org/10.1109/CSNT54456.2022.9787565>
- Lin M, Zhou S, Shao W, et al (2021) Colocated mimo radar waveform design with raised cosine filter. In: 2021 CIE International Conference on Radar (Radar). IEEE, pp 1827–1831, <https://doi.org/10.1109/RADAR53847.2021.10028103>, haikou, Hainan, China, Dec. 15–19, 2021
- Rjeb A, Seleem H, Ragheb AM, et al (2022) Raised cosine multicore fibers for high-density space division multiplexing (h-dsdm) systems. In: 2022 IEEE International Conference on Design Test of Integrated Micro Nano-Systems (DTS), pp 01–06, <https://doi.org/10.1109/DTS55284.2022.9809851>
- Simon MK, Alouini MS (1999) Bit error probability of noncoherent m-ary orthogonal modulation over generalized fading channels. *Journal of Communications and Networks* 1(2):111–117. <https://doi.org/10.1109/JCN.1999.6596754>
- Singh B, Shokeen V, Asthana R (2019) Performance evaluation of qam for improvement of ber. *Wireless Personal Communications* 109:77–88. <https://doi.org/10.1007/s11277-019-06551-3>
- Wang X, Chen HH, Liu X, et al (2025) M-ary spread multiple access and its applications in uplink cellular communications. *IEEE Transactions on Vehicular Technology* 74(4):6239–6254. <https://doi.org/10.1109/TVT.2024.3519762>
- Willstatter K, Zoltowski MD (2022) Raised-cosine frequency domain pulses for doppler-tolerant radar ambiguity functions. In: 2022 56th Asilomar Conference on Signals, Systems, and Computers. IEEE, <https://doi.org/10.1109/IEEECONF56349.2022.10051995>
- Yilmaz F, Kucur O (2009) Symbol error rate performance of qs-cdma over frequency selective time non-selective multipath generalized gamma fading channels. *Wireless Personal Communications* 49:487–516. <https://doi.org/10.1007/s11277-008-9572-4>, published online: 4 September 2008